

Disordered Yet Directed: The Emergence of Polar Flocks with Disordered Interactions

Eloise Lardet,¹ Raphaël Voituriez,^{2,3} Silvia Grigolon,^{2,*} and Thibault Bertrand^{1,†}

¹*Department of Mathematics, Imperial College London,
180 Queen's Gate, London SW7 2BZ, United Kingdom*

²*Laboratoire Jean Perrin, UMR 8237 CNRS, Sorbonne Université, 75005 Paris, France*

³*Laboratoire de Physique Théorique de la Matière Condensée,
UMR 7600 CNRS, Sorbonne Université, 75005 Paris, France*

(Dated: September 18, 2024)

Flocking is a prime example of how robust collective behavior can emerge from simple interaction rules. The flocking transition has been studied extensively since the inception of the original Vicsek model. Here, we introduce a novel self-propelled particle model with quenched disorder in the pairwise alignment interaction couplings akin to a spin glass model. We show that the presence of quenched disorder can promote (rather than destroy) the emergence of global polar order. In particular, we show that our model can display a flocking phase even when the majority of the interaction couplings are anti-aligning. Activity is the key ingredient to reduce frustration in the system as it allows local particle clustering combined with self-organization of the particles to favor neighborhoods with strong cooperative interactions.

How can simple interaction rules lead to robust and unexpected collective behavior? In statistical mechanics, paradigmatic examples are abound, from simple equilibrium spin systems to out-of-equilibrium systems of interacting self-propelled particles [1–4]. In models of self-propelled particle (SPP) systems, local consumption of energy can be used to self-organize into ordered states through local alignment interactions alone, leading to striking non-equilibrium behaviors, such as flocking [5–9]. Following earlier attempts to model flocking in animal groups [10], Vicsek et al. introduced a model of identical noisy self-propelled particles interacting solely through a local polar alignment rule akin to spins in the XY model [5]; this model displays an order-disorder phase transition [5, 11]. Interestingly, despite only having local alignment interaction rules, this model exhibits long-range order in the ordered phase in two dimensions [6, 7, 9, 12–19], as activity allows the system to escape the Mermin-Wagner-Hohenberg theorem [20, 21]. Flocking remains under intense scrutiny both theoretically [16, 22–24], and experimentally including in animal groups [8, 25, 26], bacterial colonies [27], cytoskeletal filaments driven by molecular motors [28] or synthetic colloidal systems [29–31].

Flocking has been shown to be both more robust in some respects, and more fragile in others, than originally thought. Indeed, it was recently shown to arise in the absence of explicit alignment interactions and even when these interactions should in fact prevent it [32–39]. Populations of particles with set inter- and intra-population interaction rules can display novel phases not possible in the original Vicsek model [40–43]. Conversely, although the exact details of the metric alignment rule and implementation of noise in the model do not change the asymptotic properties of the Vicsek model [44–47], the fragility of the ordered state to heterogeneity in SPP models is evident through the influence of obstacles [48–50], spatial anisotropy [51] or even dissenters [52, 53]. Discrete- and

continuous-symmetry flocks with rotational anisotropy have also recently been showed to be metastable [50, 54].

Previous works have considered extensions of the continuous-time formulation of the Vicsek model or “flying XY” model and have studied the influence of density dependent velocities [55], chirality [40, 56], and excluded volume interactions [57, 58]. Recent studies have focused on the impact of quenched and annealed random field disorder on flocks with homogeneous interaction couplings. Paradoxically, these non-equilibrium systems have been found to be more robust to quenched disorder than the corresponding equilibrium systems [59–65].

In equilibrium systems, the role of quenched disorder on phase transitions has been the subject of intense study in the context of models of disordered spins [66–69]. Disordered spin systems generically display unresolved frustration arising from the impossibility of satisfying all particle interactions at the same time. This notably leads to the so-called spin-glass phase, characterized by islands of locally aligned spins but no long-range order [69, 70]. While recent papers have explored geometrical frustration in high-density active systems [71] and nonreciprocal interactions in XY spin systems [72], our understanding of the impact of disordered alignment interactions on the emergence of flocking is still crucially lacking.

Here, we introduce the *Active Disordered XY* (ADXY) model in which disorder is quenched in the couplings, which are drawn from a Gaussian distribution, as commonly done in equilibrium spin glasses. Quenched disorder is thus introduced at the level of the couplings, a pairwise interaction property rather than a property intrinsic to the particle or the environment. Upon increasing the variance of these spin-spin couplings, we observe non-zero global polar order in systems in which there would otherwise be no long-range order [73]. Despite the fact that flocking is disrupted through other forms of coupling heterogeneity, in this case, the disorder in the couplings

surprisingly promotes, rather than destroys, flocking; activity leads to a spatial self-organization of the particles which helps decrease frustration in the system.

Active Disordered XY model. We study the dynamics of N point-like particles interacting solely via metric alignment interactions akin to an off-lattice extension of a two-dimensional disordered XY model. The particles' dynamics are governed by the following overdamped Langevin equations:

$$\dot{\mathbf{r}}_i = v_0 \hat{\mathbf{p}}_i, \quad (1a)$$

$$\dot{\theta}_i = \frac{1}{n_i} \sum_{j \in \mathcal{N}_i} K_{ij} \sin(\theta_j - \theta_i) + \eta \xi_i, \quad (1b)$$

where $\{\mathbf{r}_i, \theta_i\}$ are respectively the position and orientation of particle $i \in \{1, \dots, N\}$ at time t , n_i is the number of particles in the set of neighbors $\mathcal{N}_i = \{j : |\mathbf{r}_i - \mathbf{r}_j| \leq \sigma_I, i \neq j\}$, η is a constant noise strength and ξ_i is a Gaussian white noise with zero mean and unit variance. Particles thus move at constant speed v_0 along a self-propulsion direction $\hat{\mathbf{p}}_i = (\cos \theta_i, \sin \theta_i)$ which is subject to rotational diffusion with persistence time $\tau_p \propto \eta^{-2}$ and a polar alignment force with couplings K_{ij} from neighboring particles $j \in \mathcal{N}_i$. Our implementation of the polar forces means that the alignment is non-additive, which prevents strong clumping and is a more realistic continuous-time version of the original Vicsek model [74].

The coupling strength between each particle pair is given by K_{ij} , where $K_{ij} > 0$ gives ferromagnetic alignment and $K_{ij} < 0$ anti-ferromagnetic alignment. The couplings are independent and identically distributed quenched random variables drawn from a Gaussian distribution $K_{ij} \sim \mathcal{N}(\bar{K}, \sigma_K^2)$ with $K_{ij} = K_{ji}$ as is found in many spin glass models such as the Sherrington-Kirkpatrick (SK) model [67, 75]. In fact, in the limit of $\sigma_I \rightarrow \infty$, we recover a Langevin formulation akin to the SK model, as the spin interactions are infinite-ranged and the particle positions in Eq. (1a) are irrelevant.

In what follows, we numerically solve Eq. (1) in a square box of size L using an Euler-Maruyama method with timestep Δt . Unless stated otherwise, we use periodic boundary conditions, fix $\Delta t = 0.01$, $v_0 = 1$ and $\sigma_I = 1$, and start from initial configurations with random positions and orientations at average density $\rho = N^2/L$.

Order-disorder transition. The degree of global polar order in a flocking system is measured through the time-averaged global polar order parameter $\Psi = \langle \psi(t) \rangle_t$, where

$$\psi(t) = \frac{1}{N} \left| \sum_{i=1}^N \hat{\mathbf{p}}_i(t) \right|. \quad (2)$$

where Ψ take values from $\psi = 0$ (disorder) to $\psi = 1$ (order). Averages are taken over time (after the system reaches steady-state) as well as realizations of the random couplings K_{ij} (usually 20-50 realizations).

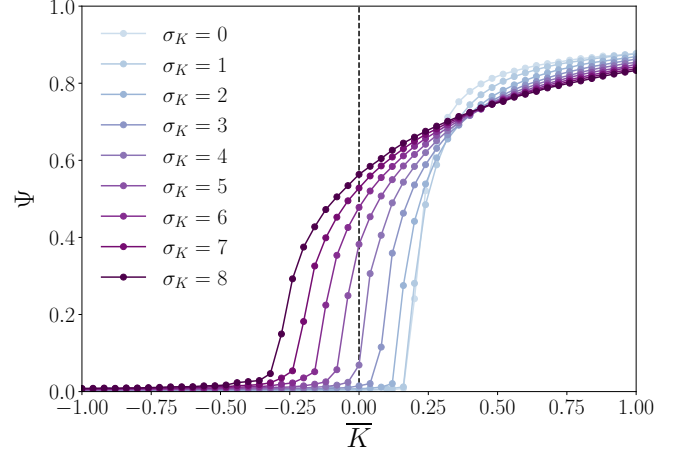


FIG. 1. Polar order parameter Ψ vs \bar{K} for increasing values of σ_K . Simulations were performed with $N = 9 \times 10^4$, $\rho = 1$, $\eta = 0.4$. The black dashed line denotes $\bar{K} = 0$.

For homogeneous couplings— $\sigma_K = 0$ and $K_{ij} = \bar{K}$ for all pairs (i, j) —a disorder-to-order phase transition is observed as the value of \bar{K} is increased [11, 55, 57, 77, 78]. We confirm this result here. For $\sigma_K > 0$, we also observe such a transition (see Fig. 1). However, as σ_K is increased, the onset of flocking strikingly shifts to negative values of \bar{K} . In the region $\bar{K} \leq 0$, order is promoted as σ_K increases, and we are able to recover a significant degree of global order, despite the fact that the majority of interactions are *anti-aligning*. In the case $\sigma_K = 0$, recent studies argue that Vicsek-type models with metric-free interactions behave as do their metric counterpart [46, 47]. Here, we confirm that our observations are robust and extend to systems with non-Gaussian distributions of random couplings and systems with topological (rather than metric) interactions (see details in [76]).

To understand the emergence of this mechanism, we compare snapshots from simulations with small and large σ_K values in Fig. 2 (see [76] for movies). To start, we consider systems with $\bar{K} = 0$, in which there are an equal number of aligning and anti-aligning interactions. At $\bar{K} = 0$ and $\sigma_K = 1$, the polar order parameter is $\Psi = 0.01$: the system is disordered and particles point in random directions [Fig. 2(a)]. Upon increasing the coupling dispersion to $\sigma_K = 8$, the steady-state polar order parameter increases to $\Psi = 0.57$. This increase in the polar order parameter corresponds to the appearance of clusters of locally aligned particles [Fig. 2(b)]. Indeed, as σ_K is increased, the distribution of number of neighbors n_i within the interaction radius becomes more right-skewed and particles are more likely to have a greater number of neighbors as shown in Fig. 2(c).

To investigate this clustering further, we look at the relationship between particle pair rescaled couplings K_{ij}/σ_K and their separation distance r_{ij} in Fig. 2(d)-(e). Owing to the Gaussian nature of the coupling distribu-

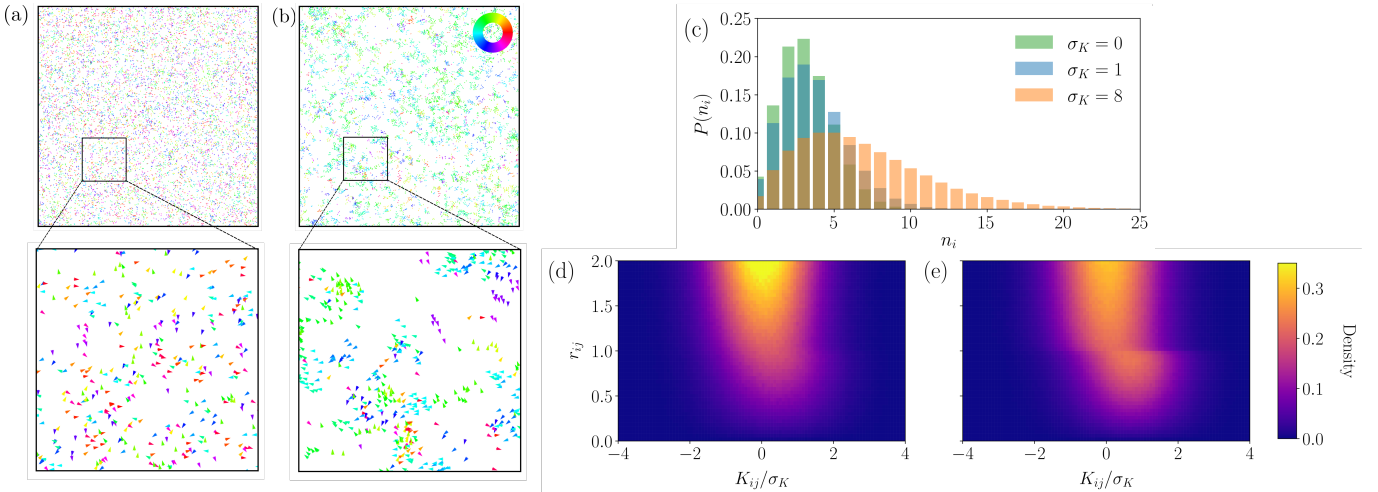


FIG. 2. Local clustering of particles. (a)-(b) Snapshots from simulations with $\sigma_K = 1$ in (a) and $\sigma_K = 8$ in (b), with $N = 10^4$, $\rho = 1$, $\eta = 0.4$, and $\bar{K} = 0$. Zoomed-in views of the simulation box are shown below with length $L/5 = 20$. The colored arrows give the particle orientations $\theta \in [0, 2\pi]$. See supplementary movies S1-S2 and their descriptions in [76]. (c) Normalized histograms for the number of neighbors n_i within the radius of interaction $\sigma_I = 1$ for the systems in (a) and (b) with $\sigma_K = 1$ in blue and $\sigma_K = 8$ in orange, as well as $\sigma_K = 0$ (non-interacting particles) in green. (d)-(e) 2D histograms of distance between particle pairs $r_{ij} = |\mathbf{r}_i - \mathbf{r}_j|$ against their coupling value for $\sigma_K = 1.0$ (d) and $\sigma_K = 8.0$ (e). Coupling values have been normalized by σ_K . Data are averaged over time (at intervals of $t = 100$ from $t = 3000$ to 3500), and realizations, with $N = 10^4$, $\rho = 1$, $\eta = 0.4$, and $\bar{K} = 0$. Note that histograms remain symmetric for values of $r_{ij} > 2$, not shown here.

tion, we would expect the joint probability distribution $P(K_{ij}/\sigma_K, r_{ij})$ to be peaked around $K_{ij}/\sigma_K = 0$ and fall off symmetrically if particles were clustered randomly. This is what we observe for distances $r_{ij} > \sigma_I$. However, for $r_{ij} < \sigma_I = 1$, we observe a clear shift towards positive coupling values, which becomes more pronounced as σ_K increases. In other words, an increase in σ_K promotes the creation of more cohesive clusters of highly aligning particles. While the quenched disorder in the couplings introduces an inherent frustration in the particle orientations, the activity allows particles to self-organize to find other particles to satisfy their interactions, thus decreasing the global frustration in the system.

Self-organization and clustering promote polar order. To systematically characterize the phases of our model, we firstly measure the polar order parameter Ψ for a fixed noise strength $\eta = 0.4$ while varying ρ , \bar{K} and σ_K [Fig. 3(a) and (d)]. Surprisingly, for large enough values of σ_K , the system exhibits a region of parameter space with global polar order but $\bar{K} \leq 0$; this is made possible thanks to the self-sorting mechanism discussed above. Note that as the density ρ is varied, we observe re-entrance in the polar order parameter not seen for homogeneous couplings ($\sigma_K = 0$); indeed, the observed critical value \bar{K}_c for the onset of flocking ($\Psi > 0$) varies non-monotonically with the density and displays a maximum around $\rho \approx 2$ for our choice of parameters.

As $\rho \rightarrow 0$, we expect a transition to disorder, as seen in the original Vicsek model [5]. At low density, the lack of interaction prevents the propagation of informa-

tion. At very high densities, particles have many interacting neighbors and the self-sorting clustering mechanism needed for polar order to arise is impaired due to a greater frustration in the system; the number of interacting neighbors outweighs the number of large, positive couplings K_{ij} , thus destroying global polar order.

To further support self-organization and clustering as a mechanism to promote polar order when $\bar{K} < 0$, we define the demixing order parameter as

$$d = \left\langle \frac{1}{N} \sum_{i=1}^N \frac{\kappa_i}{n_i} - \frac{1}{2} \right\rangle \quad (3)$$

where n_i is the total number of interacting neighbors of particle i within the radius of interaction σ_I , and κ_i is the number of interacting neighbors with $K_{ij} > 0$. Their ratio therefore quantifies the proportion of ferromagnetically interacting neighbors meaning that $d = 0$ corresponds to a perfectly mixed system and $d > 0$ (resp. $d < 0$) to a system with more local ferromagnetic (resp. anti-ferromagnetic) interactions on average. The average $\langle \cdot \rangle$ is taken over time and realizations of K_{ij} , removing particles with no neighbor from the sum.

In Fig. 3(b), we show the value of d in the (\bar{K}, ρ) -plane and draw a transition line at $d = 0$ (see Fig. 3(e) for the transitions lines for several values of σ_K). For completely mixed systems, we would expect a vertical transition lines at $\bar{K} = 0$. However, we notably find regions of parameter space where $d > 0$ despite $\bar{K} < 0$. For σ_K sufficiently large, the demixing transition lines agree well with the polar order transition [see Fig. 3(d)]. Note that

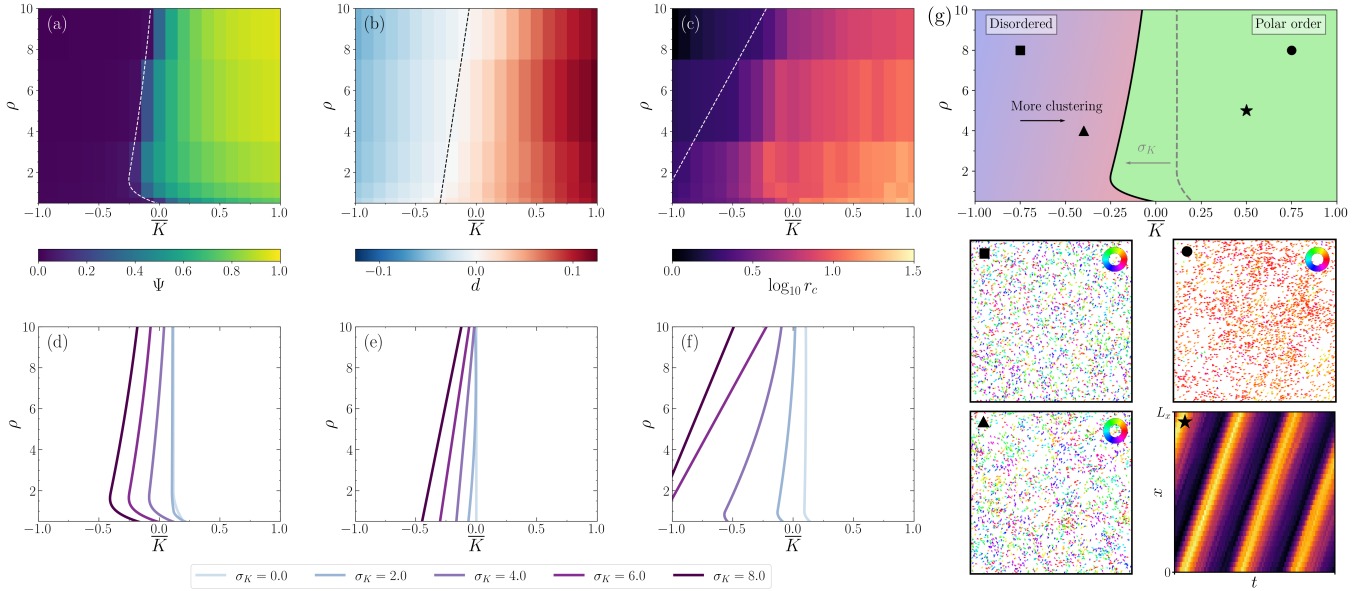


FIG. 3. Phase diagrams in the (\bar{K}, ρ) plane. (a) Color map of the polar order parameter with a dashed line showing the order-disorder transition at $\Psi = 0.1$. (b) Color map of the demixing order parameter with a dashed line for the transition at $d = 0$. (c) Color map of the clustering order parameter, with a dashed line at $r_c = 2$. For panels (a)-(c), the parameters are as follows $N = 10^4$, $\eta = 0.4$ and $\sigma_K = 6$. (d)-(f) Transition lines for various values of σ_K for the corresponding polar, demixing and clustering order parameters shown above. Transitions lines for a fixed value of $\sigma_K = 6$ are plotted on the same graph in [76]. (g) Phase diagram for $\eta = 0.4$ and $\sigma_K = 6$ based on the phases determined by the three order parameters. The gray dashed line shows the polar order transition line for $\sigma_K = 0$ (i.e. no coupling disorder). This line shifts towards the left as σ_K increases. Example snapshots from simulations are shown below (zoomed in to $L/2 \times L/2$) for $\bar{K} = -0.75$, $\rho = 8$ (square); $\bar{K} = -0.4$, $\rho = 4$ (triangle); $\bar{K} = 0.75$, $\rho = 8$ (circle). Additionally, a kymograph of the density transverse to the band's direction against time is plotted for $\bar{K} = 0.5$, $\rho = 5$ (star) with $N = 10^5$, $L_x/L_y = 5$ to show the presence of banding in the polar ordered phase. See supplementary movies S3-S6 and their descriptions in [76].

the demixing order parameter is less relevant at small densities $\rho \rightarrow 0$ as n_i is often close to zero in sparse systems. When σ_K is small, we find regions close to $\bar{K} = 0$ with $d > 0$ but $\Psi = 0$. This is likely due to the magnitude of the ferromagnetic interactions in the demixed clusters being relatively small. More highly aligning couplings are required to overcome the orientational noise and propagate information to the whole system.

For each system, we also measure the normalized equal-time connected density correlations $C_\rho(r)$ [76]. We define the typical cluster size r_c to be the radial distance such that $C_\rho(r_c) = 0.01$. In a homogeneous system, we would expect correlations to decay very quickly outside the radius of interaction, leading to $r_c \approx \sigma_I$. For systems with clustering, density fluctuations increase such that $r_c \gg \sigma_I$. Typical cluster sizes are reported on a log-scale in Fig. 3(c) for $\sigma_K = 6$. We define the boundary between homogeneous and clustered systems as $r_c = 2\sigma_I$, to discard any edge effects due to particles transiently clustering by chance. Note that the original Vicsek model ($\sigma_K = 0$) displays much weaker clustering in the disordered phase. Comparing Figs. 3(d), (e) and (f), we find regions within the disordered phase in which $r_c > 2\sigma_I$ and $\Psi = 0$, where clusters begin to appear but have not yet become demixed or large enough to display global po-

lar order. Similar disordered clustered states were found in another active particle model with distance dependent alignment [79]. Finally, note that the clustering transition observed in the disordered phase is accompanied by a transition from hyperuniform to clustered states [76].

Phase diagram for the active disordered XY model. We propose a phase diagram for the ADXY model in Fig. 3(g). For $\bar{K} \ll 0$, we have the familiar disordered homogeneous phase. As \bar{K} increases, clustering sets in. Once \bar{K} is increased further, we reach the polar ordered flocking phase, which includes regions of parameters space where $\bar{K} \leq 0$. Note that the onset of polar order is accompanied by a sharp increase in the particles persistence and the typical pairwise contact time [76].

We also find a banding phase between the disordered phase and the homogeneous polar liquid phase (or Toner-Tu phase). For $N = 10^4$, this manifests as clustered systems with large density fluctuations due to finite size effects, as shown in Fig. 2(b). However, for large enough system sizes, we recover ordered traveling bands as reported for the original Vicsek model [23]. We found our model to be subject to even stronger finite-size effects, requiring for instance even larger system sizes and a slab geometry to observe stable banding. A kymograph of the local density in slices transverse to the direction of

travel reveals clear and stable periodic bands moving in time, with the largest density close to the front of the band, leaving a density trail in its wake (see details in [76]). We believe that the nature of the order-disorder transition and the presence of long-range order remain unchanged in the ADXY model compared to the original Vicsek model (see [76] a measure of the Binder cumulant and evidence of long-range order). Finally, we observe that the flocks obtained for $\sigma_K > 0$ appear to be more fragile than those for $\sigma_K = 0$; indeed, the microscopic angular diffusion coefficient in the flocking phase is larger when quenched disorder is present at all values of \bar{K} [76].

Conclusion. In a swath of natural (including cellular tissues, bacterial suspensions, bird flocks) and synthetic (including active colloids, self-propelled bots) systems, agent-to-agent variability is the norm and we expect randomly distributed alignment interactions coupling strengths to be the rule rather than the exception. Inspired by this, we introduced the ADXY model as an extension of currently existing models of self-propelled interacting particles and showed that a transition from a disordered phase to an ordered flocking phase upon changes in density and average interaction strength. Yet, unexpectedly, we found that by increasing the standard deviation of the interaction couplings, the onset of global polar order is shifted to lower and potentially *negative* values of \bar{K} . In turn, we show that quenched disorder in the couplings can strikingly promote rather than destroy flocking, a surprising result when compared to recent studies [52, 53]. Importantly, we show that this counterintuitive phenomenon is explained by a mechanism based on clustering coupled to a self-organization by alignment interaction coupling strength: highly aligning particles can rearrange into local clusters thanks to self-propulsion therefore overcoming the local alignment frustration present in a uniform configuration. In particular, we showed that the system exhibits clustering before the onset of collective motion. Future work will attempt to explore the interplay between activity and frustration, and examine whether a spin glass phase can exist in our model and more generally in active systems. To do so, we will need to bridge analytical techniques used in active matter and spin glass theory. While the work presented here is theoretical, we believe that it will lead to a refined analysis of biological flocking systems.

We thank Hugues Chat  , Silvio Franz, Ananya Maitra, Alessandro Manacorda, Enzo Marinari, Roberto Menichetti and Francesco Zamponi for useful discussions. EL was funded by a President's PhD Scholarship at Imperial College London. SG acknowledges the ICL-CNRS fellowship and the grant Tremplin@INP by CNRS Physics as well as the hospitality of the Department of Mathematics at the Imperial College London. The authors acknowledge computing resources provided by Imperial College Research Computing Service and the Department of Mathematics Compute Cluster.

* Electronic address: silvia.grigolon@gmail.com

† Electronic address: t.bertrand@imperial.ac.uk

- [1] S. Ramaswamy, The Mechanics and Statistics of Active Matter, *Annu. Rev. Condens. Matter Phys.* **1**, 323 (2010).
- [2] M. C. Marchetti, J. F. Joanny, S. Ramaswamy, T. B. Liverpool, J. Prost, M. Rao, and R. A. Simha, Hydrodynamics of soft active matter, *Rev. Mod. Phys.* **85**, 1143 (2013).
- [3] C. Bechinger, R. Di Leonardo, H. L  wen, C. Reichhardt, G. Volpe, and G. Volpe, Active Particles in Complex and Crowded Environments, *Rev. Mod. Phys.* **88**, 045006 (2016).
- [4] M. R. Shaebani, A. Wysocki, R. G. Winkler, G. Gompper, and H. Rieger, Computational models for active matter, *Nat Rev Phys* **2**, 181 (2020).
- [5] T. Vicsek, A. Czir  k, E. Ben-Jacob, I. Cohen, and O. Shochet, Novel Type of Phase Transition in a System of Self-Driven Particles, *Phys. Rev. Lett.* **75**, 1226 (1995).
- [6] J. Toner and Y. Tu, Long-Range Order in a Two-Dimensional Dynamical XY Model: How Birds Fly Together, *Phys. Rev. Lett.* **75**, 4326 (1995).
- [7] J. Toner and Y. Tu, Flocks, herds, and schools: A quantitative theory of flocking, *Phys. Rev. E* **58**, 4828 (1998).
- [8] T. Vicsek and A. Zafeiris, Collective motion, *Physics Reports Collective Motion*, **517**, 71 (2012).
- [9] H. Chat  , Dry Aligning Dilute Active Matter, *Annual Review of Condensed Matter Physics* **11**, 189 (2020).
- [10] C. W. Reynolds, Flocks, herds and schools: A distributed behavioral model, *SIGGRAPH Comput. Graph.* **21**, 25 (1987).
- [11] G. Gr  goire and H. Chat  , Onset of Collective and Cohesive Motion, *Phys. Rev. Lett.* **92**, 025702 (2004).
- [12] Y. Tu, J. Toner, and M. Uhl, Sound waves and the absence of galilean invariance in flocks, *Phys. Rev. Lett.* **80**, 4819 (1998).
- [13] R. Aditi Simha and S. Ramaswamy, Hydrodynamic fluctuations and instabilities in ordered suspensions of self-propelled particles, *Phys. Rev. Lett.* **89**, 058101 (2002).
- [14] S. Ramaswamy, R. A. Simha, and J. Toner, Active nematics on a substrate: Giant number fluctuations and long-time tails, *Europhysics Letters* **62**, 196 (2003).
- [15] J. Toner, Y. Tu, and S. Ramaswamy, Hydrodynamics and phases of flocks, *Annals of Physics* **318**, 170 (2005), special Issue.
- [16] J. Toner, Reanalysis of the hydrodynamic theory of fluid, polar-ordered flocks, *Phys. Rev. E* **86**, 031918 (2012).
- [17] J. Toner, Birth, death, and flight: A theory of malthusian flocks, *Phys. Rev. Lett.* **108**, 088102 (2012).
- [18] A. Cavagna, L. Del Castello, S. Dey, I. Giardina, S. Melillo, L. Parisi, and M. Viale, Short-range interactions versus long-range correlations in bird flocks, *Phys. Rev. E* **92**, 012705 (2015).
- [19] B. Mahault, F. Ginelli, and H. Chat  , Quantitative Assessment of the Toner and Tu Theory of Polar Flocks, *Phys. Rev. Lett.* **123**, 218001 (2019).
- [20] N. D. Mermin and H. Wagner, Absence of Ferromagnetism or Antiferromagnetism in One- or Two-Dimensional Isotropic Heisenberg Models, *Phys. Rev. Lett.* **17**, 1133 (1966).

- [21] P. C. Hohenberg, Existence of long-range order in one and two dimensions, *Phys. Rev.* **158**, 383 (1967).
- [22] H. Chaté, F. Ginelli, G. Grégoire, and F. Raynaud, Collective motion of self-propelled particles interacting without cohesion, *Phys. Rev. E* **77**, 046113 (2008).
- [23] H. Chaté, F. Ginelli, G. Grégoire, F. Peruani, and F. Raynaud, Modeling collective motion: Variations on the Vicsek model, *Eur. Phys. J. B* **64**, 451 (2008).
- [24] A. P. Solon, H. Chaté, and J. Tailleur, From Phase to Microphase Separation in Flocking Models: The Essential Role of Nonequilibrium Fluctuations, *Phys. Rev. Lett.* **114**, 068101 (2015).
- [25] I. Giardina, Collective behavior in animal groups: Theoretical models and empirical studies, *HFSP J* **2**, 205 (2008).
- [26] A. Cavagna, I. Giardina, and T. S. Grigera, The physics of flocking: Correlation as a compass from experiments to theory, *Physics Reports The Physics of Flocking: Correlation as a Compass from Experiments to Theory*, **728**, 1 (2018).
- [27] F. Peruani, J. Starruß, V. Jakovljevic, L. Søgaard-Andersen, A. Deutsch, and M. Bär, Collective motion and nonequilibrium cluster formation in colonies of gliding bacteria, *Phys. Rev. Lett.* **108**, 098102 (2012).
- [28] V. Schaller, C. Weber, C. Semmrich, E. Frey, and A. R. Bausch, Polar patterns of driven filaments, *Nature* **467**, 73 (2010).
- [29] A. Bricard, J.-B. Caussin, N. Desreumaux, O. Dauchot, and D. Bartolo, Emergence of macroscopic directed motion in populations of motile colloids, *Nature* **503**, 95 (2013).
- [30] A. Kaiser, A. Snezhko, and I. S. Aranson, Flocking ferromagnetic colloids, *Science Advances* **3**, e1601469 (2017).
- [31] D. Geyer, A. Morin, and D. Bartolo, Sounds and hydrodynamics of polar active fluids, *Nature Materials* **17**, 789 (2018).
- [32] P. Romanczuk, I. D. Couzin, and L. Schimansky-Geier, Collective motion due to individual escape and pursuit response, *Phys. Rev. Lett.* **102**, 010602 (2009).
- [33] J. Deseigne, O. Dauchot, and H. Chaté, Collective motion of vibrated polar disks, *Phys. Rev. Lett.* **105**, 098001 (2010).
- [34] E. Ferrante, A. E. Turgut, M. Dorigo, and C. Huepe, Elasticity-based mechanism for the collective motion of self-propelled particles with springlike interactions: A model system for natural and artificial swarms, *Phys. Rev. Lett.* **111**, 268302 (2013).
- [35] M. Knežević, T. Welker, and H. Stark, Collective motion of active particles exhibiting non-reciprocal orientational interactions, *Scientific Reports* **12**, 19437 (2022).
- [36] M. Casiulis and D. Levine, Emergent synchronization and flocking in purely repulsive self-navigating particles, *Phys. Rev. E* **106**, 044611 (2022).
- [37] L. Caprini and H. Löwen, Flocking without alignment interactions in attractive active brownian particles, *Phys. Rev. Lett.* **130**, 148202 (2023).
- [38] S. Das, M. Ciarchi, Z. Zhou, J. Yan, J. Zhang, and R. Alert, Flocking by turning away, *Phys. Rev. X* **14**, 031008 (2024).
- [39] P. Baconnier, O. Dauchot, V. Démery, G. Düring, S. Henkes, C. Huepe, and A. Shee, Self-aligning polar active matter (2024), arXiv:2403.10151 [cond-mat.soft].
- [40] B. Ventejou, H. Chaté, R. Montagne, and X.-q. Shi, Susceptibility of Orientationally Ordered Active Matter to Chirality Disorder, *Phys. Rev. Lett.* **127**, 238001 (2021).
- [41] A. M. Menzel, Collective motion of binary self-propelled particle mixtures, *Phys. Rev. E* **85**, 021912 (2012).
- [42] S. Chatterjee, M. Mangeat, C.-U. Woo, H. Rieger, and J. D. Noh, Flocking of two unfriendly species: The two-species Vicsek model, *Phys. Rev. E* **107**, 024607 (2023).
- [43] R. Kürsten, J. Mihatsch, and T. Ihle, Flocking in Binary Mixtures of Anti-aligning Self-propelled Particles (2023), arxiv:2304.05476 [cond-mat].
- [44] F. Ginelli and H. Chaté, Relevance of Metric-Free Interactions in Flocking Phenomena, *Phys. Rev. Lett.* **105**, 168103 (2010).
- [45] F. Ginelli, The Physics of the Vicsek model, *Eur. Phys. J. Spec. Top.* **225**, 2099 (2016).
- [46] D. Martin, H. Chaté, C. Nardini, A. Solon, J. Tailleur, and F. Van Wijland, Fluctuation-induced phase separation in metric and topological models of collective motion, *Phys. Rev. Lett.* **126**, 148001 (2021).
- [47] D. Martin, G. Spera, H. Chaté, C. Duclut, C. Nardini, J. Tailleur, and F. van Wijland, Fluctuation-induced first order transition to collective motion (2024), arXiv:2402.05078 [cond-mat.soft].
- [48] O. Chepizhko, E. G. Altmann, and F. Peruani, Optimal Noise Maximizes Collective Motion in Heterogeneous Media, *Phys. Rev. Lett.* **110**, 238101 (2013).
- [49] A. Morin, N. Desreumaux, J.-B. Caussin, and D. Bartolo, Distortion and destruction of colloidal flocks in disordered environments, *Nature Phys.* **13**, 63 (2017).
- [50] J. Codina, B. Mahault, H. Chaté, J. Dobnikar, I. Pagonabarraga, and X.-q. Shi, Small Obstacle in a Large Polar Flock, *Phys. Rev. Lett.* **128**, 218001 (2022).
- [51] A. Solon, H. Chaté, J. Toner, and J. Tailleur, Susceptibility of Polar Flocks to Spatial Anisotropy, *Phys. Rev. Lett.* **128**, 208004 (2022).
- [52] G. Baglietto, E. V. Albano, and J. Candia, Gregarious versus individualistic behavior in Vicsek swarms and the onset of first-order phase transitions, *Physica A: Statistical Mechanics and its Applications* **392**, 3240 (2013).
- [53] D. Yllanes, M. Leoni, and M. C. Marchetti, How many dissenters does it take to disorder a flock?, *New Journal of Physics* **19**, 103026 (2017).
- [54] B. Benvenuto, O. Granek, S. Ro, R. Yaacoby, H. Chaté, Y. Kafri, D. Mukamel, A. Solon, and J. Tailleur, Metastability of discrete-symmetry flocks, *Phys. Rev. Lett.* **131**, 218301 (2023).
- [55] F. D. C. Farrell, M. C. Marchetti, D. Marenduzzo, and J. Tailleur, Pattern Formation in Self-Propelled Particles with Density-Dependent Motility, *Phys. Rev. Lett.* **108**, 248101 (2012).
- [56] B. Liebchen and D. Levis, Collective behavior of chiral active matter: Pattern formation and enhanced flocking, *Phys. Rev. Lett.* **119**, 058002 (2017).
- [57] A. Martín-Gómez, D. Levis, A. Díaz-Guilera, and I. Pagonabarraga, Collective motion of active Brownian particles with polar alignment, *Soft Matter* **14**, 2610 (2018).
- [58] Y. Zhao, T. Ihle, Z. Han, C. Huepe, and P. Romanczuk, Phases and homogeneous ordered states in alignment-based self-propelled particle models, *Phys. Rev. E* **104**, 044605 (2021).
- [59] F. Peruani and I. S. Aranson, Cold active motion: How time-independent disorder affects the motion of self-propelled agents, *Phys. Rev. Lett.* **120**, 238101 (2018).
- [60] J. Toner, N. Guttenberg, and Y. Tu, Swarming in the Dirt: Ordered Flocks with Quenched Disorder, *Phys.*

- Rev. Lett. **121**, 248002 (2018).
- [61] J. Toner, N. Guttenberg, and Y. Tu, Hydrodynamic theory of flocking in the presence of quenched disorder, Phys. Rev. E **98**, 062604 (2018).
- [62] Y. Duan, B. Mahault, Y.-q. Ma, X.-q. Shi, and H. Chaté, Breakdown of Ergodicity and Self-Averaging in Polar Flocks with Quenched Disorder, Phys. Rev. Lett. **126**, 178001 (2021).
- [63] L. Chen, C. F. Lee, A. Maitra, and J. Toner, Packed swarms on dirt: Two-dimensional incompressible flocks with quenched and annealed disorder, Phys. Rev. Lett. **129**, 188004 (2022).
- [64] L. Chen, C. F. Lee, A. Maitra, and J. Toner, Hydrodynamic theory of two-dimensional incompressible polar active fluids with quenched and annealed disorder, Phys. Rev. E **106**, 044608 (2022).
- [65] L. Chen, C. F. Lee, A. Maitra, and J. Toner, Incompressible polar active fluids with quenched random field disorder in dimensions $d > 2$, Phys. Rev. Lett. **129**, 198001 (2022).
- [66] S. F. Edwards and P. W. Anderson, Theory of spin glasses, Journal of Physics F: Metal Physics **5**, 965 (1975).
- [67] D. Sherrington and S. Kirkpatrick, Solvable Model of a Spin-Glass, Phys. Rev. Lett. **35**, 1792 (1975).
- [68] K. Binder and A. P. Young, Spin glasses: Experimental facts, theoretical concepts, and open questions, Rev. Mod. Phys. **58**, 801 (1986).
- [69] K. H. Fischer and J. A. Hertz, *Spin Glasses*, Cambridge Studies in Magnetism (Cambridge University Press, Cambridge, 1991).
- [70] M. Mezard, G. Parisi, and M. Virasoro, *Spin Glass Theory and Beyond* (World Scientific, 1986).
- [71] M. Paoluzzi, D. Levis, and I. Pagonabarraga, From flocking to glassiness in dense disordered polar active matter, Commun Phys **7**, 1 (2024).
- [72] R. Hanai, Nonreciprocal Frustration: Time Crystalline Order-by-Disorder Phenomenon and a Spin-Glass-like State, Phys. Rev. X **14**, 011029 (2024).
- [73] Indeed, no long-range order would be observed in a Vicsek model with a non random couplings whose value is set to the same average coupling strength.
- [74] O. Chepizhko, D. Saintillan, and F. Peruani, Revisiting the emergence of order in active matter, Soft Matter **17**, 3113 (2021).
- [75] S. Kirkpatrick and D. Sherrington, Infinite-ranged models of spin-glasses, Phys. Rev. B **17**, 4384 (1978).
- [76] See Supplemental Material at [] for further analytical and computational details, including supplementary movies. See also references [80–82] therein.
- [77] G. Grégoire, H. Chaté, and Y. Tu, Moving and staying together without a leader, Physica D: Nonlinear Phenomena **181**, 157 (2003).
- [78] E. Sese-Sansa, I. Pagonabarraga, and D. Levis, Velocity alignment promotes motility-induced phase separation, EPL **124**, 30004 (2018), arxiv:1807.07497 [cond-mat].
- [79] R. Großmann, P. Romanczuk, M. Bär, and L. Schimansky-Geier, Pattern formation in active particle systems due to competing alignment interactions, Eur. Phys. J. Spec. Top. **224**, 1325 (2015).
- [80] P. Jentsch and C. F. Lee, A new universality class describes Vicsek's flocking phase in physical dimensions (2024), arxiv:2402.01316 [cond-mat, physics:physics].
- [81] H. Chaté and A. Solon, Dynamic Scaling of Two-Dimensional Polar Flocks (2024), arxiv:2403.03804 [cond-mat].
- [82] S. Torquato, Hyperuniform states of matter, Physics Reports **745**, 1 (2018).

Supplemental Material for “Disordered Yet Directed: The Emergence of Polar Flocks with Disordered Interactions”

Eloise Lardet,¹ Raphaël Voituriez,^{2,3} Silvia Grigolon,^{2,*} and Thibault Bertrand^{1,†}

¹*Department of Mathematics, Imperial College London,
180 Queen’s Gate, London SW7 2BZ, United Kingdom*

²*Laboratoire Jean Perrin, UMR 8237 CNRS, Sorbonne Université, 75005 Paris, France*

³*Laboratoire de Physique Théorique de la Matière Condensée,
UMR 7600 CNRS, Sorbonne Université, 75005 Paris, France*

(Dated: September 18, 2024)

CONTENTS

I. Supplementary movies	1
II. Confirming the phase transition	2
A. Weighted bimodal coupling distribution	2
B. Topological interactions	3
III. Density fluctuations correlations	3
IV. Hyperuniformity in the ADXY model	4
V. Distribution of pairwise contact times	5
VI. Banding persists in the ADXY model	7
VII. Nature of the phase transition and ordered phase	8
A. Binder cumulant	8
B. Long-range order	9
VIII. Angular MSD	9
References	10

I. SUPPLEMENTARY MOVIES

We provide supplementary movies accompanying Fig. 2 and Fig. 3 of the main text. Particle orientation polar histograms are included alongside the particle trajectories for Movies S1-S5. Movie S6 shows an example movie of banding.

The parameters used are given as follows:

- Movie S1: $N = 10^4$, $\rho = 1$, $\eta = 0.4$, $\bar{K} = 0$, and $\sigma_K = 1$.
- Movie S2: $N = 10^4$, $\rho = 1$, $\eta = 0.4$, $\bar{K} = 0$, and $\sigma_K = 8$.
- Movie S3: $N = 10^4$, $\rho = 8$, $\eta = 0.4$, $\bar{K} = -0.75$, and $\sigma_K = 6$.
- Movie S4: $N = 10^4$, $\rho = 4$, $\eta = 0.4$, $\bar{K} = -0.4$, and $\sigma_K = 6$.
- Movie S5: $N = 10^4$, $\rho = 8$, $\eta = 0.4$, $\bar{K} = 0.75$, and $\sigma_K = 6$.
- Movie S6: $N = 10^5$, $\rho = 5$, $\eta = 0.4$, $\bar{K} = 0.5$, and $\sigma_K = 6$, in a slab geometry with $L_x/L_y = 5$.

* Electronic address: silvia.grigolon@gmail.com

† Electronic address: t.bertrand@imperial.ac.uk

II. CONFIRMING THE PHASE TRANSITION

In the main text, we provided phase diagrams for the ADXY model with normally distributed interaction couplings and metric interactions. Here, we further provide in Fig. S1 a surface plot of the order-disorder transition in the space $(\bar{K}, \sigma_K, \rho)$ for $\eta = 0.4$. We clearly see the presence of re-entrant behavior with increasing σ_K .

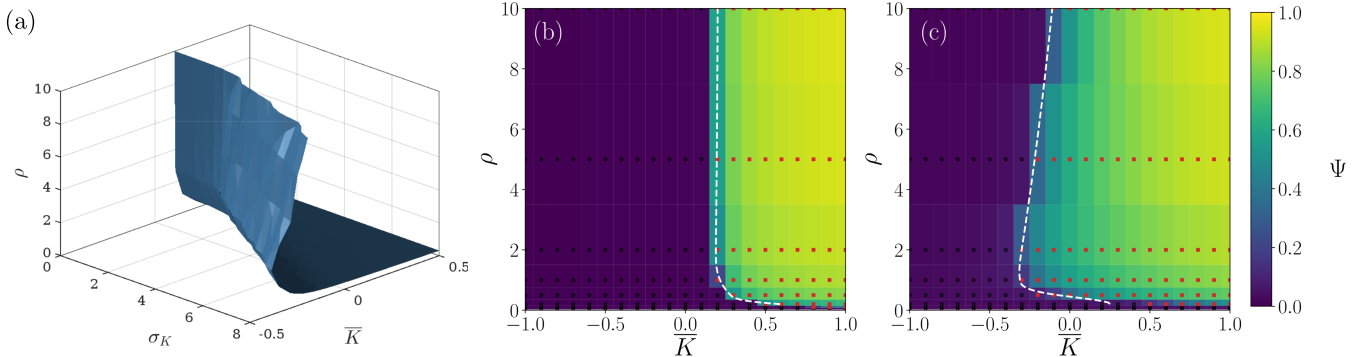


FIG. S1. Order-disorder phase transition in the ADXY model. (a) Surface plot for boundary between disordered and ordered polar phase. (b)-(c) 2d phase plot slices of (a) for $\sigma_K = 0$ (b) and $\sigma_K = 8$ (c). The white dashed lines show the boundaries between the disordered and ordered polar phase. Simulations were performed with $N = 10^4$, $\eta = 0.4$.

We also combine in a single phase diagram the three transition lines described in Fig. 3 of the main text.

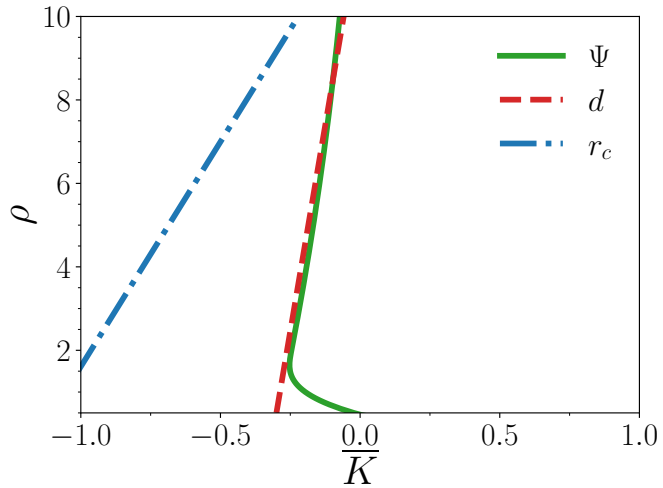


FIG. S2. Transition lines in the ADXY model for a single value of $\sigma_K = 6$ including the transition lines defined through the global order parameter Ψ , the demixing order parameter d and the typical cluster size r_c as measured using local density correlation functions. Simulations were performed with $N = 10^4$, $\eta = 0.4$.

To confirm their robustness, we also confirmed that our results remain qualitatively unchanged for a different interaction coupling distribution and if topological interactions are used instead of metric ones.

A. Weighted bimodal coupling distribution

First, we modify the coupling distribution while maintaining the first two moments of the original Gaussian coupling distribution. We introduce a weighted bimodal coupling distribution such that couplings only take one of two distinct values. Specifically, we consider a probability distribution with two modes K_+ and K_- , such that K_+ is chosen with

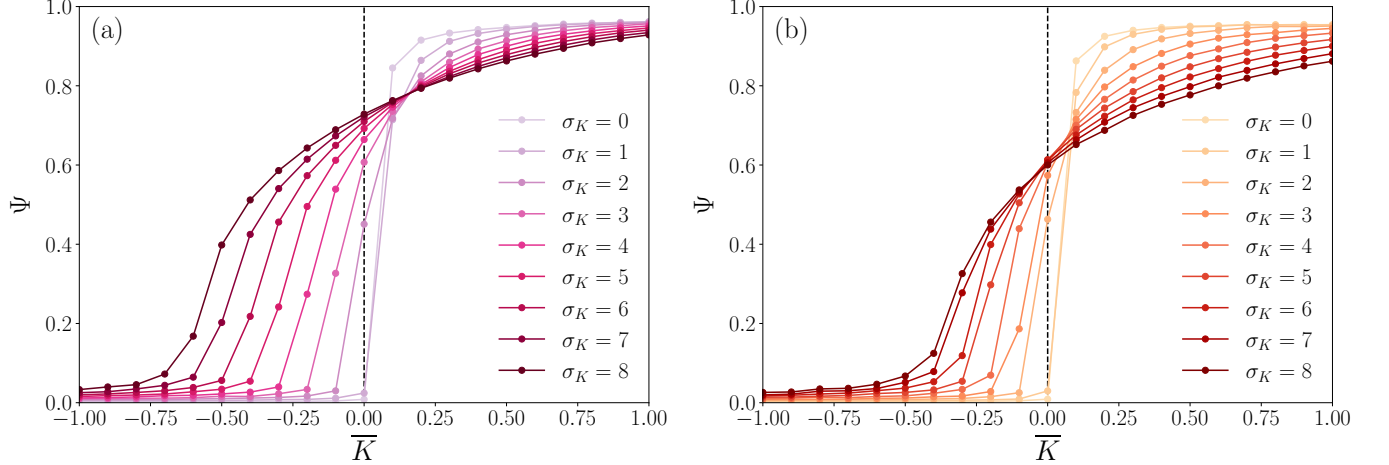


FIG. S3. Polar order parameter Ψ vs \bar{K} for increasing σ_K with (a) weighted bimodal couplings or (b) topological interactions. Simulations were performed with $N = 10^4$, $\rho = 1$, and $\eta = 0.2$. The interaction range is $\sigma_I = 1$ in (a) and $k = 7$ neighbors in (b). The black dashed lines show the vertical line $\bar{K} = 0$.

probability α . We can easily write down the mean and standard deviation of this distribution:

$$\bar{K} = \alpha K_+ + (1 - \alpha) K_-, \quad (\text{S1})$$

$$\sigma_K = (1 + K_+) \sqrt{\alpha(1 - \alpha)}. \quad (\text{S2})$$

If we fix \bar{K}, σ_K , and α , it is simple to calculate the values of K_+ and K_- :

$$K_+ = \bar{K} + \sigma_K \sqrt{\frac{1 - \alpha}{\alpha}}, \quad (\text{S3})$$

$$K_- = \bar{K} - \sigma_K \sqrt{\frac{\alpha}{1 - \alpha}}. \quad (\text{S4})$$

To relate this distribution to a Gaussian distribution with the same \bar{K} and σ_K , we can choose α such that this is equal to the probability that $K_{ij} > 0$ in the Gaussian distribution $\mathcal{N}(\bar{K}, \sigma_K)$, which can be calculated through a simple integration:

$$\alpha \equiv \int_0^\infty \frac{1}{\sigma_K \sqrt{2\pi}} e^{-\frac{1}{2} \left(\frac{x - \bar{K}}{\sigma_K} \right)^2} dx. \quad (\text{S5})$$

Implementing this distribution in our model with reciprocal couplings, we show the phase transitions in Fig. S3 as a function of \bar{K} for various values of σ_K . As σ_K is increased, we see the same shift of the onset of flocking to negative \bar{K} as in the Gaussian coupling distribution model as in Fig. S1.

B. Topological interactions

Secondly, we use topological interactions with k nearest neighbors, rather than metric interaction range as in the main text. To do so, we simply redefine the interaction neighbors of each particle \mathcal{N}_i to be the k -nearest neighbors, in terms of the L_2 norm. We show the phase transition for this case in Fig. S3(b) as a function of \bar{K} as σ_K increases. Again, we clearly see the same shift of the onset of flocking to negative \bar{K} as σ_K increases, just as in the main text.

III. DENSITY FLUCTUATIONS CORRELATIONS

To quantify clustering in the system, we calculate density fluctuations correlations. Specifically, we coarse-grain the system into discrete boxes with length $\ell = 1$, and calculate local number densities $\rho(\mathbf{r}, t)$ within each box, where \mathbf{r} is

defined as the center of the box. We calculate the density fluctuations $\delta\rho(\mathbf{r}, t) = \rho(\mathbf{r}, t) - \langle \rho(\mathbf{r}, t) \rangle_{\mathbf{r}}$. The equal-time connected density correlation function is given by

$$C_{\rho}(r) = \frac{\langle \delta\rho(\mathbf{r}_i, t) \cdot \delta\rho(\mathbf{r}_i + \mathbf{r}, t) \rangle_{\mathbf{r}_i, t}}{\langle |\delta\rho(\mathbf{r}_i, t)|^2 \rangle_{\mathbf{r}_i, t}}. \quad (\text{S6})$$

This has been normalized such that $C_{\rho}(0) = 1$. To speed up computation time, correlations were calculated using a Fast Fourier Transform (FFT). We plot C_{ρ} against radial distances $r = |\mathbf{r}|$. We do not concern ourselves with measuring this in the directions perpendicular and parallel to the mean heading direction, as we are mainly concentrating on the transition between a disordered homogeneous system and small clusters appearing, which we expect to be isotropic.

Example correlation functions are shown in Fig. S4 at fixed $\sigma_K > 0$ and ρ for increasing \bar{K} , across the order-disorder transition. When plotted on a log-log scale, we see that for intermediate values of r , these correlation functions follow a power law scaling. We further observe an exponential cutoff for large values of r due to finite size effects. As described in the main text, we define r_c to be the radial distance such that density fluctuations correlations have decayed enough, i.e. $C_{\rho}(r_c) = 0.01$, and use this to estimate the typical cluster size in the system. This value was chosen as it signifies that the correlations have sufficiently decayed, but is also measured in the algebraic scaling regime so that measurements are not skewed by the exponential cut-off.

As \bar{K} increases, the value of r_c increases, indicating the size of clusters are increasing. Despite the system being disordered at $\bar{K} = -0.5$ ($\Psi \approx 0$), the system still shows clustering with $r_c \approx 4$, defining a *disordered but clustered* phase.

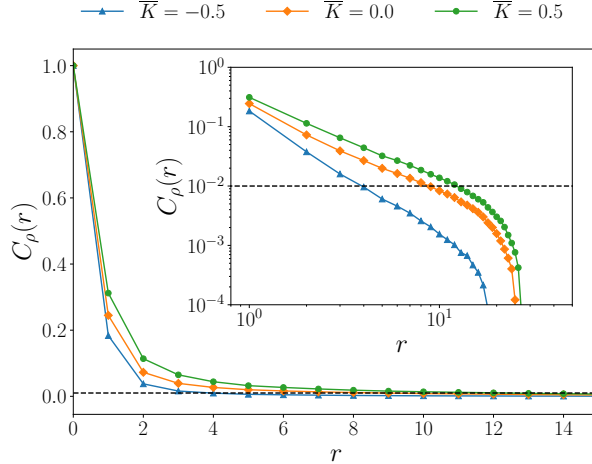


FIG. S4. Density fluctuation correlation functions for $\sigma_K = 6$, $\rho = 1$, and $\bar{K} \in \{-0.5, 0.0, 0.5\}$. These are shown on a linear scale in the main figure and on a log-log scale in the inset. Correlations were averaged over time and realizations through a linear binning in r . A black dashed line is shown at $C_{\rho}(r) = 0.01$ to indicate the value at which r_c is defined.

IV. HYPERNIFORMITY IN THE ADXY MODEL

Motivated by our findings of regions of larger density fluctuations and clustering within the disordered phase of the model, we study further the statistics of density fluctuations. In line with literature on hyperuniformity [1], we measure the variance of the local density $\sigma^2(\rho_{\ell})$, where ρ_{ℓ} is the density of particles found in the region of volume $V = \ell^d$. The average is taken over many different volumes of the same system as well as different configurations.

We expect the variance of the local density to scale with the size of the probing window such that

$$\sigma^2(\rho_{\ell}) \sim \ell^{-\lambda} \quad (\text{S7})$$

For Poisson point processes, we expect that the scaling exponent $\lambda = d$ (here, $d = 2$). If $\lambda > d$, then the density fluctuations are decaying faster than for a uniform system, such a system is called hyperuniform. Finally, if $\lambda < d$, then one observes enhanced density fluctuations, the system is structured in space, and we can call our system clustered.

As can be seen in Fig. S5, the configurations obtained in the disordered phase display density fluctuations characterized by an exponent λ varying from $\lambda > 2$ to $\lambda < 2$ as the typical cluster size as measured from the density correlation functions increases. We confirm the existence of a transition from *hyperuniform* to *clustered* configurations in the disordered phase by plotting in Fig. S6 the values of λ measured via a power-law fit.

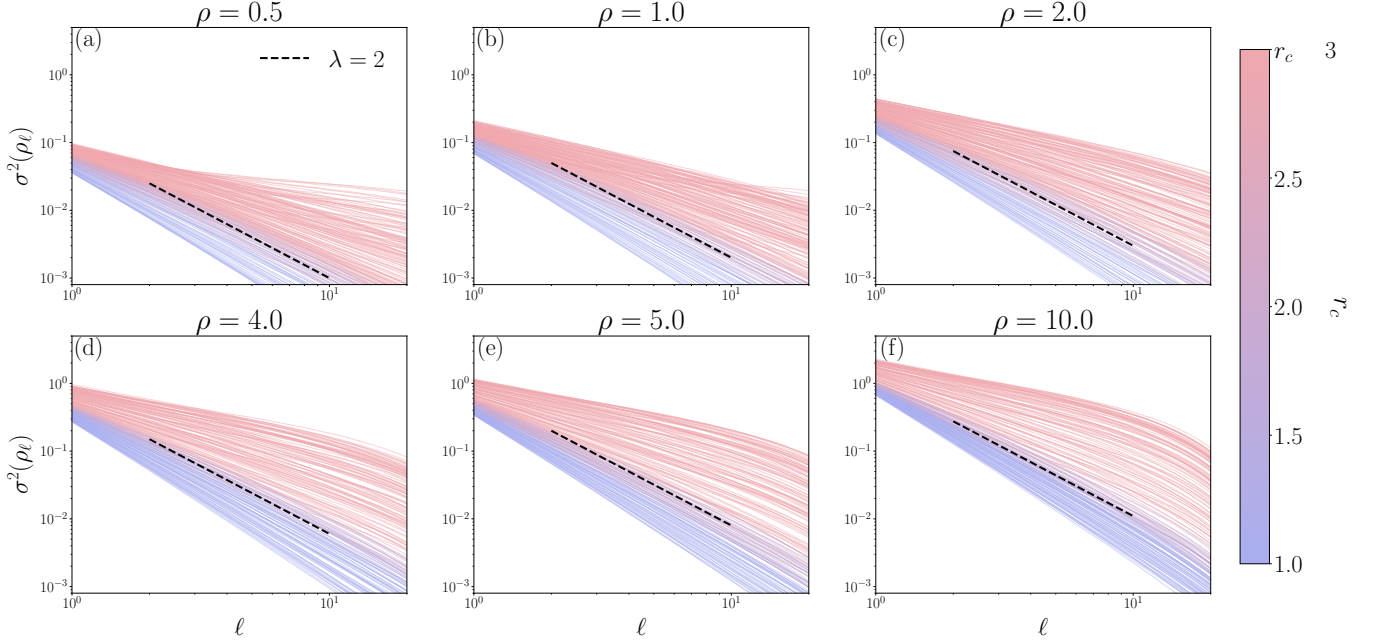


FIG. S5. Density variance $\sigma^2(\rho_\ell)$ vs ℓ for each of $\rho \in \{0.5, 1, 2, 4, 5, 10\}$ in (a)-(f). In each subplot, the lines are plotted for $\bar{K} \in \{-1.0, -0.9, \dots, 1.0\}$ and $\sigma_K \in \{0, 1, 2, \dots, 8\}$. Each curve is here colored according to the value of r_c as measured from the density correlation functions. A dashed black line is shown for exponent $\lambda = 2$. Other simulation parameters were $N = 10^4$, $\eta = 0.4$, and 10^4 sample observation windows of the final simulation snapshot in steady state were taken for 20 realizations for each value of ℓ to obtain the variance.

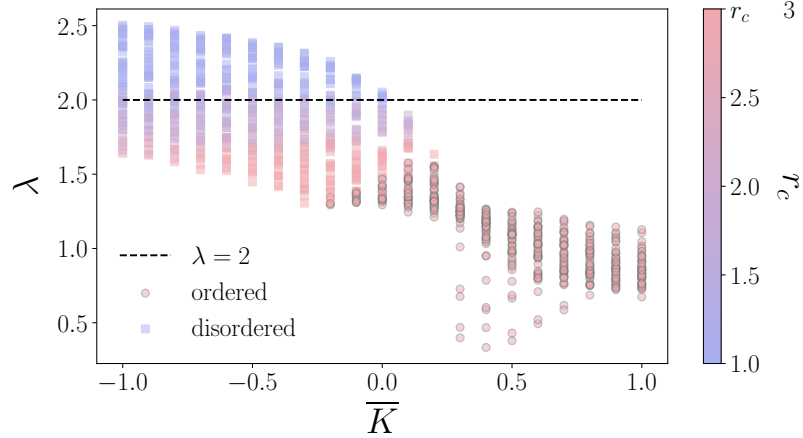


FIG. S6. Power law exponent fitted from density variance $\sigma^2(\rho_\ell) \sim \ell^{-\lambda}$ for $2 \leq \ell \leq 10$ as a function of \bar{K} . All points are plotted with $\rho \in \{0.5, 1, 2, 4, 5, 10\}$ and $\sigma_K \in \{0, 1, 2, \dots, 8\}$. Each point is here colored according to its value of r_c as measured from the density correlation functions. Squares are obtained in the disordered phase ($\Psi < 0.1$) and circles are configurations in the ordered phase ($\Psi > 0.1$). A dashed black line shows the exponent $\lambda = 2$ for uniform systems. Other simulation parameters were $N = 10^4$, and $\eta = 0.4$.

V. DISTRIBUTION OF PAIRWISE CONTACT TIMES

We define the pairwise contact time to be the total number of snapshots in which particles i and j are within distance r_{\max} of each other, over a certain period of time. In this way, we can define the percentage of time in contact as

$$\tau_{ij} = \sum_{t=1}^{N_T} H(r_{\max} - |\mathbf{r}_i(t) - \mathbf{r}_j(t)|)/N_T \quad (\text{S8})$$

where N_T is the total number of snapshots, and $H(r)$ is the Heaviside step function. By construction, our pairwise contact time lies in the range $\tau \in [0, 1]$.

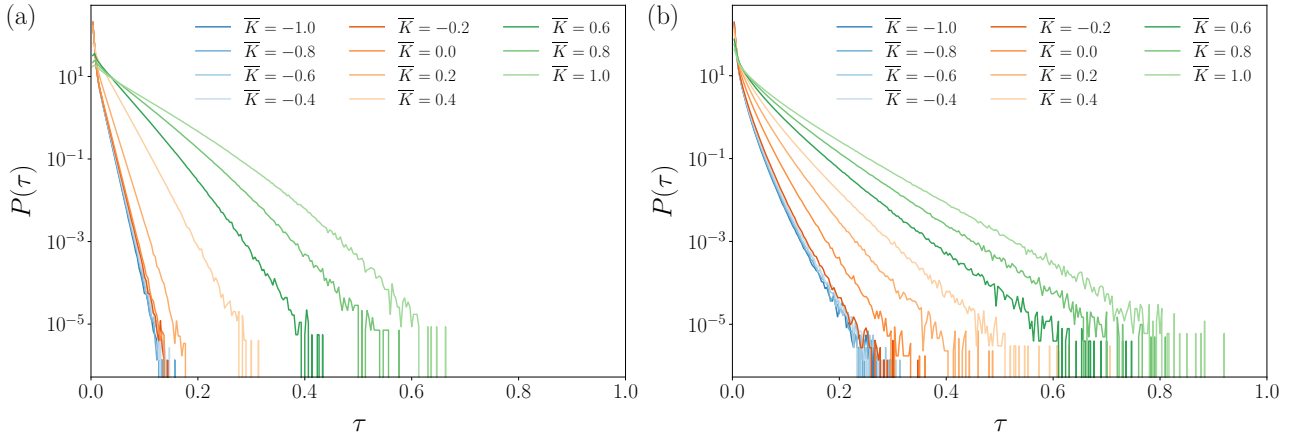


FIG. S7. Pairwise contact time distributions for (a) $\sigma_K = 0$, $\rho = 4$ and (b) $\sigma_K = 6$, $\rho = 4$.

We find that the pairwise contact times as defined above are distributed exponentially (see Fig. S7). By fitting the distributions to an exponential distribution $e^{-\tau/\lambda}$, we can extract from the data typical pairwise contact times. We measure over intermediate values of τ to avoid any skew from very short random scattering events as well as outliers with large contact times. The exponents are plotted for $r_{\max} = 1$ in Fig. S8. Here, we denote \bar{K}_c the value of the mean coupling strength at which the system transitions from disordered to ordered. We find that pairwise contact time distributions remain unchanged throughout the disordered phase ($\bar{K} - \bar{K}_c < 0$); in the ordered phase ($\bar{K} - \bar{K}_c > 0$), the typical pairwise contact time increases as the mean coupling strength increases for all values of σ_K .

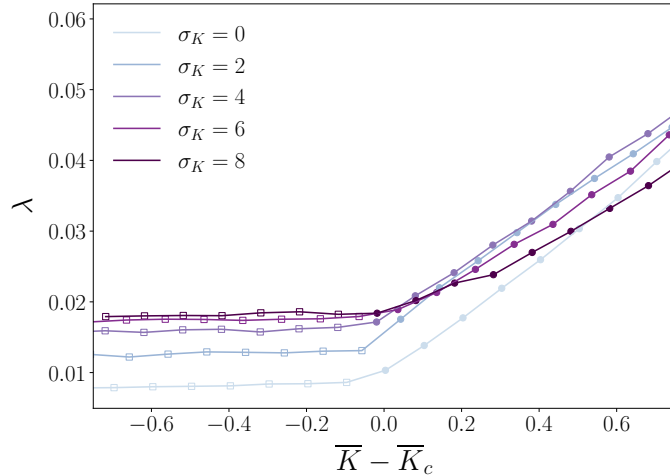


FIG. S8. Exponent measured from the probability distributions of pairwise contact times $P(\tau)$ as a function of the distance to the critical average coupling strength \bar{K}_c . To obtain λ , exponential functions of the form $\sim e^{-\tau/\lambda}$ were fitted between the 20th and 80th percentile of unique nonzero τ values measured. Empty squares denote systems with no polar order ($\Psi < 0.1$) and filled circles denote systems with polar order ($\Psi \geq 0.1$), in line with the phase diagram in main text Fig. 3. Simulations were performed with $N = 10^4$, $\rho = 4$, $\eta = 0.4$, $\sigma_K = 6$, and $r_{\max} = 1$.

As a further measure to compare the probability density functions of contact times, we measure the Kullback-Lieber (KL) divergence for $P_{\bar{K}, \sigma_K}(\tau)$ using as reference the distribution observed for the system furthest into the disordered phase at a given σ_K ($\bar{K} = -1$ here). Here, the KL divergence is thus defined as

$$D_{KL}(\bar{K}, \sigma_K) = \sum_{\tau, P(\tau) \neq 0} P_{\bar{K}, \sigma_K}(\tau) \log \left(\frac{P_{\bar{K}, \sigma_K}(\tau)}{P_{-1, \sigma_K}(\tau)} \right) \quad (\text{S9})$$

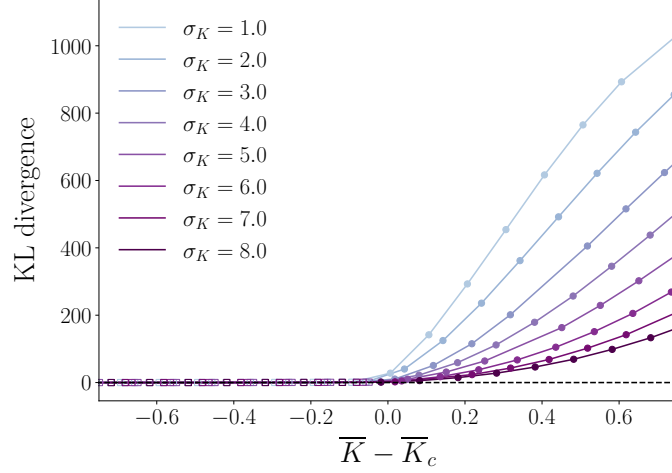


FIG. S9. KL divergence for percentage contact time probability distributions $P(\tau)$ compared against the baseline of $\bar{K} = -1.0$ and the same value of \bar{K} . Empty squares denote systems with no polar order ($\Psi < 0.1$) and filled in circles for systems with polar order ($\Psi \geq 0.1$), in line with the phase diagram in main text Fig. 3. Simulations were performed with $N = 10^4$, $\rho = 4$, $\eta = 0.4$, and $r_{\max} = 1$.

where we stipulate that the sum must only be measured over percentage contact times τ such that $P_{-1,\sigma_K}(\tau)$ and $P_{\bar{K},\sigma_K}(\tau)$ are both nonzero. The divergence is zero if the distributions are identical over this range of τ , and positive nonzero otherwise. We clearly see in Fig. S9 that the KL divergence remains very close to zero for all values of mean coupling strength such that $\bar{K} - \bar{K}_c < 0$. The KL divergence then increases monotonically with mean coupling strength in the ordered phase.

VI. BANDING PERSISTS IN THE ADXY MODEL

As noted in the main text, we still observe a coexistence phase in the ADXY model in which the system displays ordered bands. These are, however, subject to large finite-size effects. To confirm their existence, we had to simulate large systems in a slab geometry when $\sigma_K > 0$.

In Fig. S10, we analyze the effect of increasing σ_K on the bands, at fixed \bar{K} and ρ . We have used a large noise value

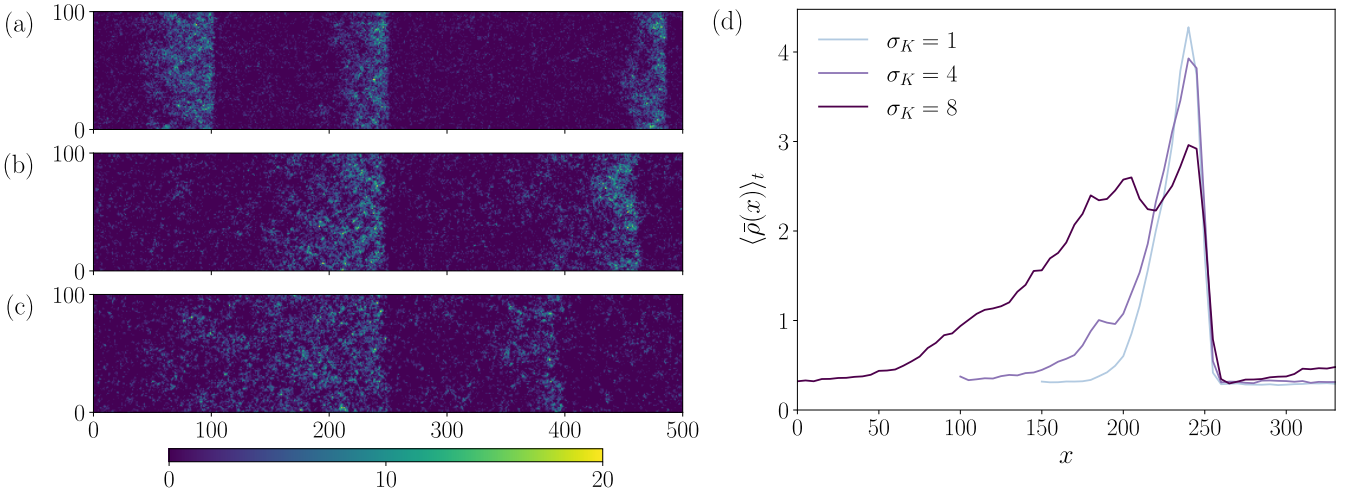


FIG. S10. Banding for increasing σ_K . (a)-(c) Snapshots of the coarse-grained densities in the coexistence phase for $\sigma_K = 1$, 4 and 8, respectively. (d) Density profiles perpendicular to the direction of travel, averaged over time at intervals of $t = 10$ from $t = 5000$ to 6000. Simulations were performed with $N = 5 \times 10^4$, $L_x = 500$, $L_y = 100$, $\rho = 1$, $\eta = 0.7$, $\bar{K} = 1$.

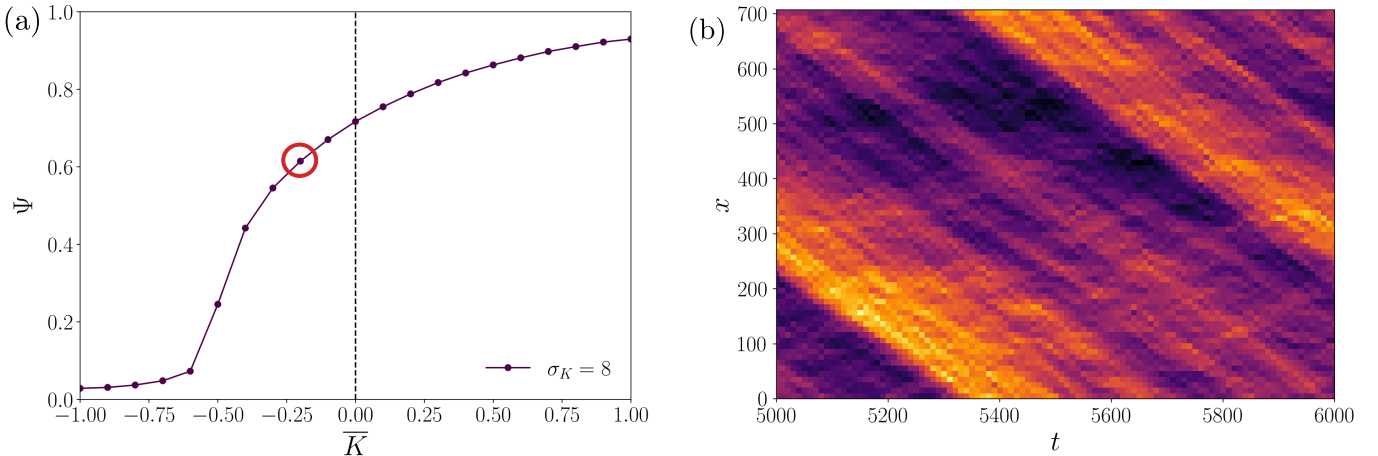


FIG. S11. Banding for $\bar{K} < 0$. (a) Polar order parameter Ψ against \bar{K} for $N = 10^4$, $\rho = 1$, $\eta = 0.2$, and $\sigma_K = 8$. The point at $\bar{K} = -0.2$ is circled in red to highlight where we look for banding. (b) Kymograph of the local density in slices transverse to the direction of travel against time. This shows a clear, linear periodic band moving in time. Simulations for (b) were performed with $N = 10^5$ and $L_x/L_y = 5$.

of $\eta = 0.7$, as bands are observed for all values of σ_K studied here; in this case, we find clear and stable bands and are able to average over their transverse density profiles, shown in Fig. S10(b). As σ_K increases, the band wavelength increases, and the density inside the band decreases. The density of the bands need to decrease in order to sufficiently spread out the highly aligning clusters. Otherwise, this would cause frustration and break apart the bands into a disordered phase.

At $\eta = 0.7$, the transition to polar order occurs at $\bar{K} > 0$. We therefore wish to verify that bands are still observed in polar ordered regions close to the transition when $\bar{K}_c < 0$, which we can achieve by decreasing η and making σ_K large enough. We choose $\eta = 0.2$ to ensure the region $\bar{K} < 0$ is sufficiently deep in the banding phase to see clear bands. However, as noise decreases, the difference in density within and outside the bands becomes even smaller. At the same time, we saw that a higher σ_K causes the bands to spread out and wavelength increases. We therefore plot kymographs of the transverse density against time to provide a clearer picture for the moving bands when σ_K is large and η is small. With large enough systems, we can see clear signatures of banding in the kymograph when $\bar{K} < 0$, see Fig. S11.

VII. NATURE OF THE PHASE TRANSITION AND ORDERED PHASE

A. Binder cumulant

The original Vicsek model assumed that the transition from order to disorder was of second-order [2]. Later, Grégoire and Chaté proved that this observation was due to finite-size effects and that this transition is in fact of first-order [3] by simulating much larger systems and measuring the Binder cumulant:

$$G = 1 - \frac{\langle \psi^4 \rangle}{3 \langle \psi^2 \rangle^2}. \quad (\text{S10})$$

The Binder cumulant involves the fourth moment of the order parameter (kurtosis), thus quantifying the sharpness of a line. First-order phase transitions are characterized by a discontinuous jump in the order parameter as the control parameter is varied. A negative dip in the Binder cumulant for large enough system size is a strong indication of a first-order, discontinuous transition. In our model with small $\sigma_K > 0$, we observe a $G < 0$ dip around the transition point of $\bar{K}_c \approx 0.48$ as \bar{K} is increased (see Fig. S12(a)). For this set of parameter values, the transition point is at a positive value of \bar{K} . However, for larger σ_K and lower η , the transition is shifted to negative values of \bar{K} . Here, we were not yet able to find this negative dip in G ; it may be that much larger system sizes and a much finer resolution in terms of \bar{K} is required here to clearly see the discontinuity. However, the presence of bands, as discussed in the previous section, is further evidence of a first-order transition [4]. We thus believe that the order of the transition in unaffected by the addition of the quench disorder in the interaction coupling strengths.

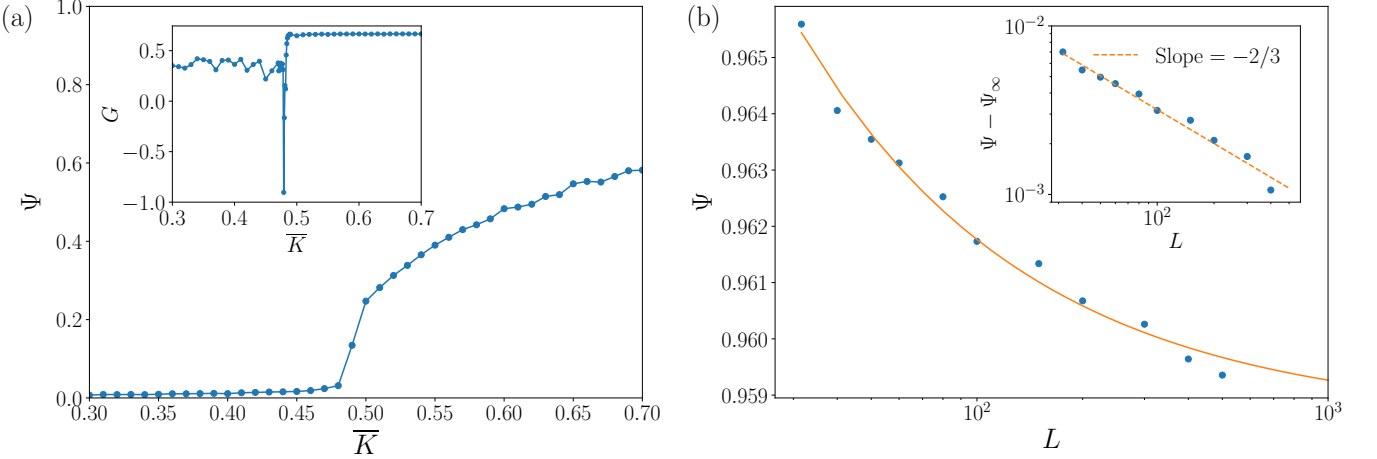


FIG. S12. Nature of the phase transition and ordered phase. (a) Polar order parameter Ψ vs \bar{K} with $\sigma_K = 1$. Inset: Binder cumulant G vs \bar{K} with a negative dip around the transition point. Simulations were performed with $N = 6 \times 10^4$, $\rho = 1$, and $\eta = 0.6$. (b) Polar order parameter Ψ vs system size L with a line showing a fitted curve, which has algebraic decay to an asymptotic value of $\Psi_\infty = 0.958(5)$ and a scaling exponent of $\omega = -2/3$. The inset shows the log-log fit of $\Psi - \Psi_\infty \sim L^\omega$ in a dashed line for the data (blue dots). Simulations were performed with $\rho = 1$, $\eta = 0.2$, $\bar{K} = 1$, $\sigma_K = 1$.

B. Long-range order

The discovery of this disorder-induced polar order brings into question the nature of the global polar order. One of the most surprising results of the Vicsek model was that it shows long-range polar order in $d = 2$, apparently breaking the Mermin-Wagner-Hohenberg theorem. This was confirmed analytically by Toner and Tu using hydrodynamic theories, proving that the liquid phase of polar flocks shows true long-range order [5].

Numerically, this can be verified by a decay of the order parameter slower than a power law with the size of the system L , with algebraic decay to a constant asymptotic value of Ψ_∞ [4] with the scaling $\Psi - \Psi_\infty \sim L^\omega$. A theoretical value of $\omega_{TT} = -2/3$ was predicted by Toner and Tu [6–9].

Due to computing resources limitations (namely, storing the interaction coupling strengths demands a lot of memory and reaching a steady-state when N is large takes much longer), we have not been able to simulate systems larger than $L = 500$. Nevertheless, we have been able to confirm true long-range order in the polar ordered phase of our model for $\sigma_K = 1$ by plotting the global polar order against system size in Fig. S12(b). We find that our data is well-fitted by $\Psi = cL^\omega + \Psi_\infty$, where c is a constant, ω is a scaling exponent and Ψ_∞ is the predicted asymptotic value of Ψ as $L \rightarrow \infty$. Here, we find that $\Psi_L - \Psi_\infty \sim L^\omega$ with $\omega = -0.51 \pm 0.10$ but as can be seen in the inset the theoretical exponent also seems to describe well the data; more data is required to reach a meaningful conclusion. This evidence suggests that the model with quenched coupling disorder still shows true long-range order in the liquid phase.

VIII. ANGULAR MSD

Finally, we measure a time-averaged angular mean squared displacement (MSD) for each particle, before averaging over particles, realizations and time for each realization

$$\langle \Delta\theta^2 \rangle(t) = \left\langle \frac{1}{N} \sum_{i=1}^N \theta_i(t + \tau) - \theta_i(\tau) \right\rangle_\tau \quad (\text{S11})$$

For sufficiently large t , we expect to observe rotational diffusion consistent with the following scaling $\langle \Delta\theta^2 \rangle = 2D_\theta t$, where D_θ is the effective angular diffusion coefficient. We plot both the angular MSD over time and the long-time effective diffusion coefficients in Fig. S13, comparing $\sigma_K = 0$ and $\sigma_K = 6$. By varying \bar{K} across the polar order-disorder transition, we see that D_θ is roughly constant within the disordered phase and begins to decrease at the transition point as we enter the polar ordered phase for both $\sigma_K = 0$ and $\sigma_K = 6$. We also observe that diffusion coefficients are uniformly smaller for $\sigma_K = 0$ across the whole range of \bar{K} tested. We thus conclude that flocks are more fragile (particles are overall less persistent in direction) when quenched disorder is added in the interaction couplings.

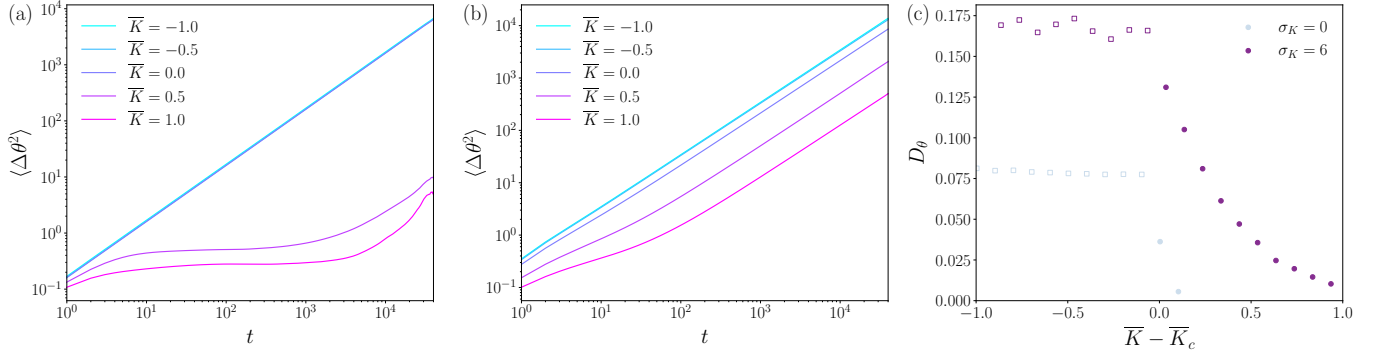


FIG. S13. (a) Mean angular MSD for various values of \bar{K} for fixed $\sigma_K = 0$. (b) Mean angular MSD for various values of \bar{K} for fixed $\sigma_K = 6$. (c) Effective diffusion coefficient by measuring D_θ from a linear fit over the interval $t \in [10^3, 10^4]$ for various values of $\bar{K} - \bar{K}_c$ and $\sigma_K = 0, 6$. Empty squares denote systems with no polar order ($\Psi < 0.1$) and filled in circles for systems with polar order ($\Psi \geq 0.1$), in line with the phase diagram in main text Fig. 3. Simulations were performed with $N = 10^4$, $\rho = 4$, $\eta = 0.4$, $\sigma_K = 6$, and were run to $t = 4 \times 10^4$.

- [1] S. Torquato, Hyperuniform states of matter, *Physics Reports* **745**, 1 (2018).
- [2] T. Vicsek, A. Czirók, E. Ben-Jacob, I. Cohen, and O. Shochet, Novel Type of Phase Transition in a System of Self-Driven Particles, *Phys. Rev. Lett.* **75**, 1226 (1995).
- [3] G. Grégoire and H. Chaté, Onset of Collective and Cohesive Motion, *Phys. Rev. Lett.* **92**, 025702 (2004).
- [4] H. Chaté, Dry Aligning Dilute Active Matter, *Annual Review of Condensed Matter Physics* **11**, 189 (2020).
- [5] J. Toner and Y. Tu, Long-Range Order in a Two-Dimensional Dynamical XY Model: How Birds Fly Together, *Phys. Rev. Lett.* **75**, 4326 (1995).
- [6] J. Toner and Y. Tu, Flocks, herds, and schools: A quantitative theory of flocking, *Phys. Rev. E* **58**, 4828 (1998).
- [7] Toner and Tu predicted the connected, equal-time, velocity autocorrelation to scale $C(r) \propto r^{2\chi/\zeta}$ for sufficiently large r , with $\chi = -1/5$, $\zeta = 3/5$ in $d = 2$. However, these scaling exponents were later shown not to be exact [10]. This exponent was found to be approximately -0.65 by others later numerically [11].
- [8] P. Jentsch and C. F. Lee, A new universality class describes Vicsek's flocking phase in physical dimensions (2024), arxiv:2402.01316 [cond-mat, physics:physics].
- [9] H. Chaté and A. Solon, Dynamic Scaling of Two-Dimensional Polar Flocks (2024), arxiv:2403.03804 [cond-mat].
- [10] J. Toner, Reanalysis of the hydrodynamic theory of fluid, polar-ordered flocks, *Phys. Rev. E* **86**, 031918 (2012).
- [11] B. Mahault, F. Ginelli, and H. Chaté, Quantitative Assessment of the Toner and Tu Theory of Polar Flocks, *Phys. Rev. Lett.* **123**, 218001 (2019).